FOI

Depth sounding lidar model with multipixel receiver

MICHAEL TULLDAHL

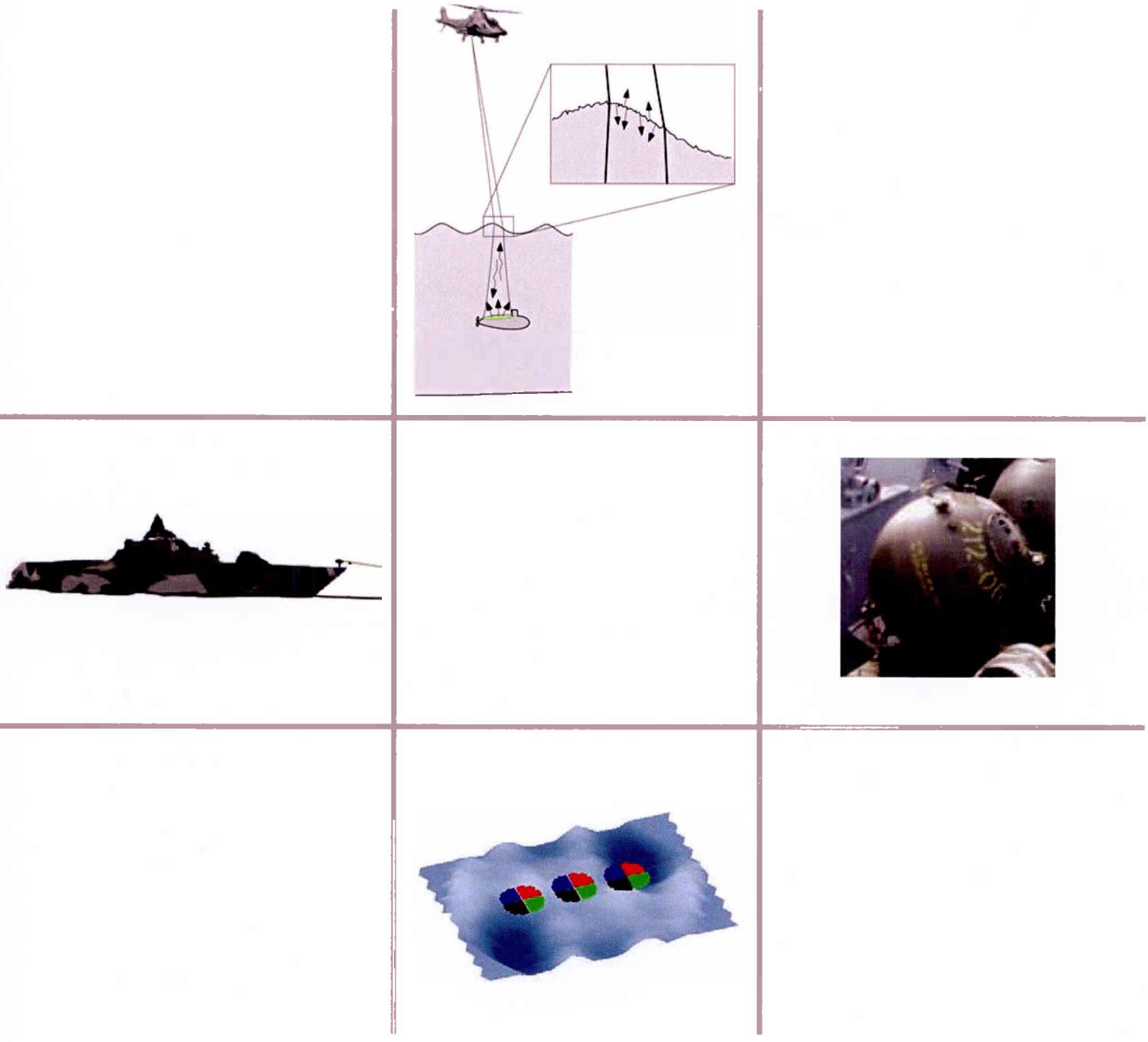

FOI-R--2074--SE Technical report
ISSN 1650-1942 September 2006

Systems Technology

Michael Tulldahl

Depth sounding lidar model with multipixel receiver

FOI-R--2074--SE
ISSN 1650-1942

Technical report
September 2006

Systems Technology

Issuing organization	Report number, ISRN	Report type
FOI – Swedish Defence Research Agency Systems Technology SE-164 90 Stockholm	FOI-R--2074--SE	Technical report
	Research area code 4. C4ISTAR	
	Month year September 2006	**Project no.** E6058
	Sub area code 43 Underwater Surveillance, Target acquistion and Reconnaissance	
	Sub area code 2	

Author/s (editor/s)	Project manager
Michael Tulldahl	Henrik Claesson
	Approved by
	Sponsoring agency Swedish Armed Forces
	Scientifically and technically responsible Michael Tulldahl

Report title

Depth sounding lidar model with multipixel receiver

Abstract

In this report we present a theoretical model for depth sounding lidar (light detection and ranging) with the ability to simulate modern multipixel lidar receivers with several detectors. The model is valuable for target signature studies, performance estimation of target detection, estimation of surface wave signals and development of signal processing for water volume turbidity estimation or sea bottom classification. The modeling results are exemplified with two simple configurations of a four-pixel lidar receiver. The theoretical results show that signals from a multipixel system can be used to estimate the local sea surface slope angle within one laser shot. The results also show that a sea surface correction factor could be applied to improve the estimation of the sea bottom properties from the bottom echo and that the use of specific pixel information for certain pixel geometries can improve the performance for target detection when the detection is limited by the volume backscatter signal. The multipixel lidar model uses a ray-tracing method that accounts for transmission through a sea surface with both large and small scale waves (ripples) as well as multiple scattering of the laser pulse within the water volume.

Keywords

signatures, multiple scattering, underwater sensors, remote sensing, surface waves, lidar

Further bibliographic information	Language English

ISSN 1650-1942	Pages 24 p.
	Price acc. to pricelist

Utgivare	Rapportnummer, ISRN	Klassificering
FOI - Totalförsvarets forskningsinstitut Systemteknik 164 90 Stockholm	FOI-R--2074--SE	Teknisk rapport
	Forskningsområde 4. Ledning, informationsteknik och sensorer	
	Månad, år September 2006	**Projektnummer** E6058
	Delområde 43 Undervattenssensorer	
	Delområde 2	

Författare/redaktör	Projektledare
Michael Tulldahl	Henrik Claesson
	Godkänd av
	Uppdragsgivare/kundbeteckning Försvarsmakten
	Tekniskt och/eller vetenskapligt ansvarig Michael Tulldahl

Rapportens titel

Modell för djupsonderande lidar med flerpixelmottagare

Sammanfattning

I denna rapport presenteras en modell för simulering av djupsonderande lidar (light detection and ranging) med flerpixelmottagare. Modellen är ett verktyg för studier av mål- och vaksignaturer, detektionsprestanda, skattning av ytekosignal och för utveckling av algoritmer för mätning av skiktning i vatten och bottenklassificering. Modellresultaten exemplifieras med två olika konfigurationer av 4-pixelmottagare. De teoretiska resultaten indikerar att signalerna från flerpixelmottagare kan användas för att göra skattningar av våglutningen där laserskottet träffar vattenytan. Resultaten visar också att en korrektionsfaktor kan användas för att förbättra skattningen av bottenparametrar från bottenekosignalen samt att användningen av specifik pixelinformation kan förbättra prestanda för måldetektion i de fall då detektionen begränsas av bakåtspridning från vattenvolymen. Den utvecklade flerpixelmodellen använder ray-tracingmetoder som tar hänsyn till multipelspridning av laserpulsen i vattnet samt till vågor på vattenytan med våglängder ned till krusningars storlek.

Nyckelord

signaturer, multipel spridning, undervattenssensorer, fjärrsensorer, ytvågor, lidar

Övriga bibliografiska uppgifter	Språk Engelska
ISSN 1650-1942	**Antal sidor:** 24 s.
Distribution enligt missiv	**Pris: Enligt prislista**

Contents

1. Introduction

In this report we present a theoretical model for depth sounding lidar (light detection and ranging). The purpose of the model is to predict the lidar pulse response from airborne and mast-mounted lidar sensors. The specific work presented is this report concerns the model capacity to simulate modern multipixel lidar receivers with several detectors. The work is an extension of our earlier modeling efforts.[1] The ability to simulate multipixel systems is important for many purposes such as performance estimation for target detection, target signature and wake signature studies, estimation of surface wave signals and development of signal processing for water volume turbidity estimation or sea bottom classification. We exemplify the results with two different configurations of a lidar receiver with four pixels. However, simulations can be performed with an arbitrary number of pixels in the receiver with the available simulation time as the only limitation. Simulations of active (for example gated viewing) and passive (video) imaging systems are possible but for more than 100-1000 pixels, the computation burden becomes too high. The simulation time for one pixel is from 1 s to 1 min depending on the required accuracy and water depth.

A depth sounding lidar can be used for depth measurements and target detection. The airborne lidar has proven to be a valuable sensor for depth sounding with its possibilities for rapid and accurate sounding of shallow areas. An illustration of the measurement principle is shown in Fig. 1 and an example of target detection in Fig. 2. An example of a reflected and received pulse response waveform of a transmitted laser pulse is shown in Fig. 1 (b). The received signal in the lidar system is time-resolved and the bottom depth is calculated from the time interval between the sea surface and the bottom reflections. The backscatter from the water volume shows an approximately exponential decay with increasing depth z within the waveform. The measurement principle for a mast-mounted lidar is similar to an airborne lidar. A mast-mounted lidar can be used for detection and obstacle warning on a ship or for detection of shallow underwater targets mounted on a fixed mast, for example in a harbor or on a bridge, see Fig. 3 and Fig. 4.

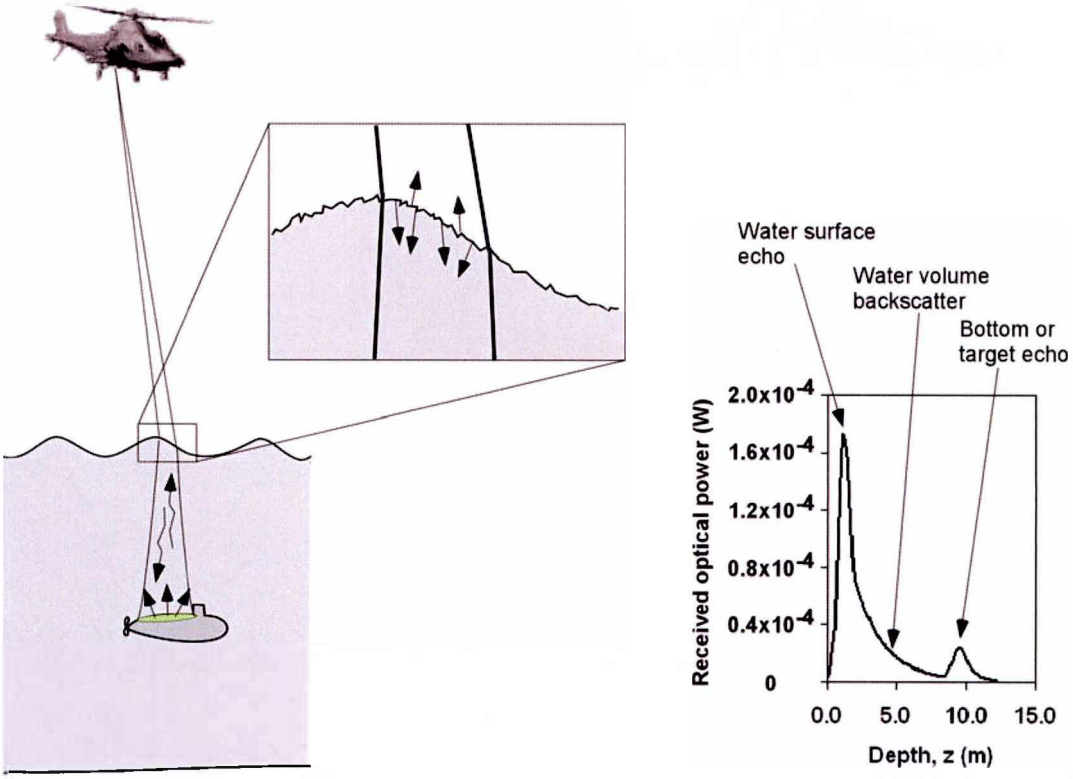

Fig. 1. Illustration of an airborne depth sounding lidar (a) and an example of a received waveform (b).

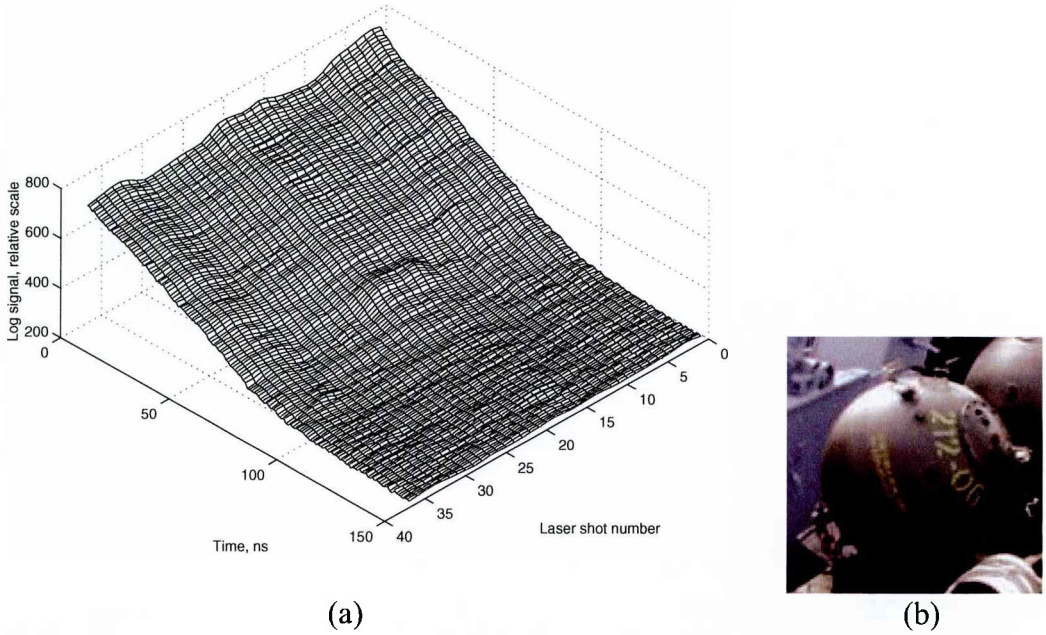

Fig. 2. Experimental example of airborne detection of a spherical mine dummy at 9 m depth, with the Hawk Eye I system. Target echoes from the mine can be seen in the middle of the waveform plot (a). The mine dummy used in the experiment[2] is shown in figure (b) and has a diameter of 1 m.

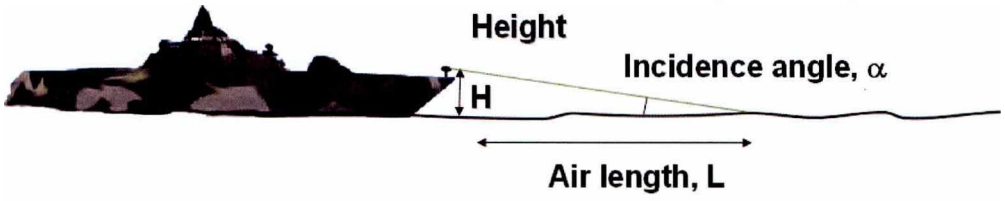

H = 3 m		H = 5 m		H = 8 m	
α (°)	L (m)	α (°)	L (m)	α (°)	L (m)
20	8	20	14	20	22
15	11	15	19	15	30
10	17	10	28	10	45
8	21	8	36	8	57
6	29	6	48	6	76
4	43	4	72	4	114
2	86	2	143	2	229

Fig. 3. Schematic illustration of a mast mounted lidar system for detection of shallow underwater targets. Various incidence angles and air ranges are exemplified for different mast heights above the sea surface.

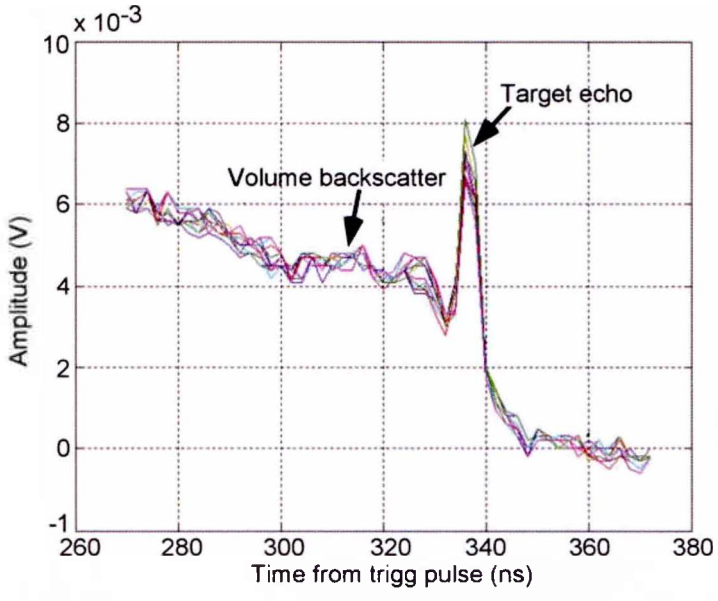

Fig. 4. Example of an echo from a 1 m^2 target 1 m below the sea surface. The data is from an experiment with a mast-lidar with incidence angle α = 5.4° to the sea surface (cf. Fig. 3).

2. Multipixel lidar model

We will use the multipixel lidar model for description of an airborne system. A schematic illustration of the lidar measurement system and its typical parameter values are given in Fig. 5 and in Table 1 respectively. The significant system parameters are the laser output pulse energy E_0, the FWHM laser pulse length t_0, laser beam divergence, flight altitude H, transmitter optical efficiency η_{Tx}, and incident beam off-nadir angle θ_0. The receiver parameters are the one-dimensional field of view (FOV), optical efficiency η_{Rx} and the receiver aperture area A_R. For a flat water

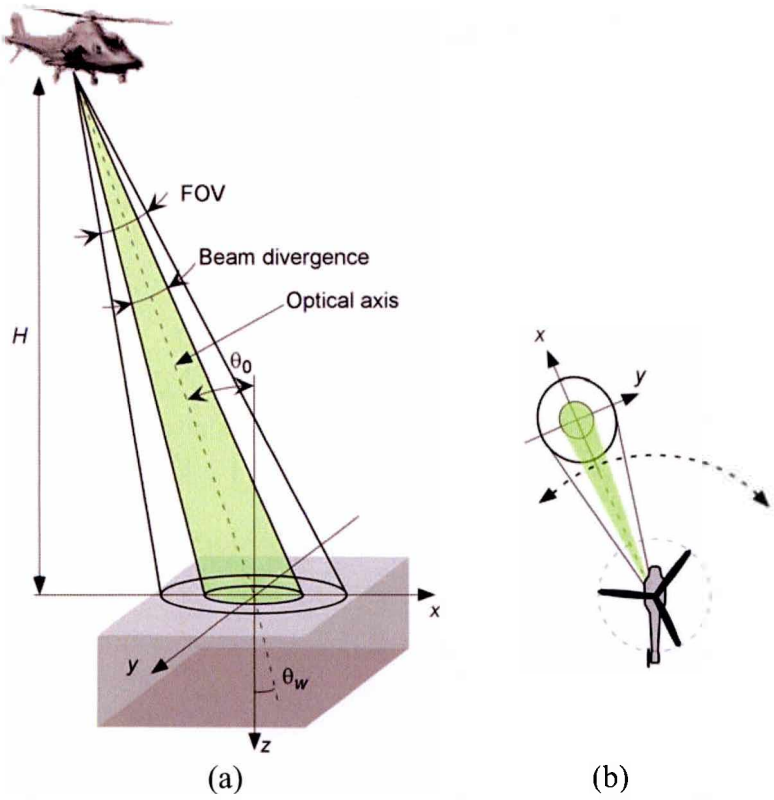

Fig. 5. Schematic illustration of the depth sounding lidar system and the (x, y, z)-coordinate system. The coordinate system has its origin in the hit on the mean water surface level by the optical axis of the collocated, collinear transmitter and receiver. The laser inclination angle θ_0 is in the x-z plane.

Table 1. Parameters and typical values for airborne depth sounding lidar.

Laser system	**Value**	**Unit**
Pulse energy (λ = 532 nm) (E_0)	5	mJ
Beam off-nadir angle (θ_0)	20	°
Flight altitude (H)	200	m
Laser beam divergence, Gaussian beam full width with irradiance decreased to $e^{-1/2}$	10–15	mrad
Pulse length (FWHM) (t_0)	5	ns
Optical efficiency (η_{Tx})	0.9	
Receiver system		
Aperture area (A_R)	0.025	m^2
Field of view, full angle (FOV)	10–50	mrad
Optical efficiency (η_{Rx})	0.9	
Atmosphere		
Two-way atmospheric loss (T_{atm}^2)	0.9	
Target or bottom		
Target or bottom reflectivity (ρ_t)	0.1	

surface, the off-nadir angle in water is $\theta_w = \arcsin\{\sin(\theta_0)/n_w\}$, where $n_w = c_0/c_w$, and c_0 and c_w are the velocities of light in air and water, respectively. The laser beam footprint diameter on the sea surface is typically about 1–2 m and the receiver field-of-view larger than 2 m. A scanner sweeps the beam and FOV in a semi-arc pattern with a nearly constant off-nadir angle θ_0. For an airborne sensor, a nearly constant nadir angle gives the advantage of a nearly constant slant range and a uniform spot density. The nadir angle and slant range are used for depth bias and wave height corrections to obtain accurate depth estimation.

2.1 Modeling method

The simulation model consists of components for calculation of laser pulse transfer through the sea surface, pulse propagation within the water and reflection on the sea bottom or targets. The pulse transfer through the sea surface is calculated using a triangular grid, Fig. 6 (b), which resolves the *large-scale* surface waves. The incident power from the laser beam and the receiver response in its field-of-view are divided into local rays on each surface triangle. These local rays are reflected from or transferred through the surface triangles using a model for small-scale waves or *ripples* (capillary waves). The capillary wave model is generated as precalculated look-up tables, called for in each transfer through a surface triangle. The surface wave pattern has several impacts on the lidar signal; especially the sea surface echo strength depends on the specific large and small scale wave pattern for each lidar shot. The in-water beam propagation and reflection on the sea bottom or targets are calculated with beam tracing and analytical beam propagation functions. A detailed description of each model component is given in Ref. 1. In the following we will briefly describe how the pulse response is calculated.

The received backscatter from the water column is calculated as a weighted sum of individual impulse responses for each pair of transmitter and receiver rays on the surface triangles. The weighting factor for an individual impulse response is given by the product of the transmitted power through the entrance triangle and the receiver response factor of the exit triangle. Thus, each sea surface triangle (Fig. 6 (b)) is used in the context of both a transmitter and a receiver. For calculation of the target or bottom echo a similar triangular grid as the water surface is used. The geometry and significant parameters for the backscatter calculation from *one* transmitter-receiver triangle-pair is shown in Fig. 7. The impulse response for one triangle-pair is affected by:

- Triangle separation.
- Initial beam width (corresponding to the triangle grid size).
- Initial beam divergence (corresponding to the scattering in the water surface).
- Propagated beam width from beam spreading due to scattering within the water.
- Angle between optical axes of the rays through the two surface triangles.

The analytical functions used for the impulse response calculation for one triangle-pair is described in Ref. 3. By summing the individual impulse responses, the important characteristics of the backscatter can be calculated with respect to water parameters and different parameter settings in the lidar system such as the off-nadir angle, the beam width and the receiver field-of-view. All of these parameters

influence the backscatter and target returns both in total backscattered energy and the temporal distribution of the received radiation. The propagated beam width due to scattering in water is calculated with analytical beam spread function developed by McLean *et al.*[4] Examples of water *optical* parameters of importance for the received backscatter are:

- The absorption coefficient (absorbed energy per unit distance of propagation). The approximately exponential decay of the volume backscatter in Fig. 1 (b) is explained by the absorption of backscattered energy from each depth z.
- The scattering coefficient (scattered energy per unit distance of propagation, affecting the beam broadening). The beam broadening affects the intersection between the transmitter and the receiver beams (Fig. 7) and also causes a temporal stretching of the transmitted and reflected laser pulse.
- The backscattering coefficient (backscattered energy per unit distance of propagation). The amount of backscattered energy from each depth z is proportional to the backscattering coefficient at depth z.

2.2 Horizontally stratified water volume

For calculation of the received pulse response (backscatter) from a horizontally stratified water column we have modified the calculations for the propagated beam width to account e.g. for the increased beam width when the beam passes through a layer with increased scattering coefficient. The calculations are made in the small angle approximation,[4] meaning that mean scattering angles are close to zero and that errors in the solution can occur if that is not the case.

We have also considered the increased slant depth that is due to the oblique incidence of the transferred rays. The oblique incidence (see example in Fig. 6 (b)) of a transferred optical axis is of importance for appropriate calculation of the temporal distribution of the backscattered energy from a certain depth. If the correct geometrical distances are not calculated, a scattering layer in the water volume may be shown too clearly in the simulated waveform and consequently the possibility to detect the layer in the lidar signal will be overestimated. An additional modification made in the simulation model concerns the depth-averaging of the absorption coefficient. With this modification the backscattered radiation from depth z is subject to an absorption calculated from the actual distance traveled upwards in each layer from depth z.

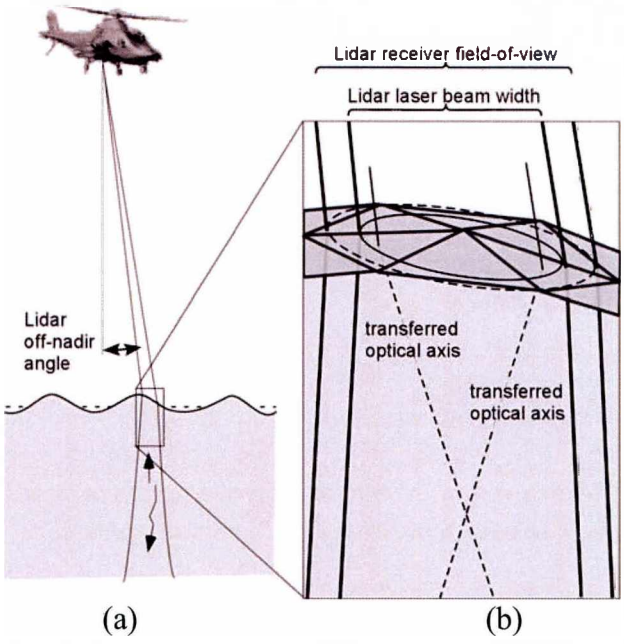

Fig. 6. Illustration of the depth sounding lidar system (a). The laser beam (solid) and the receiver (dashed) footprints are illustrated as ellipses on the sea surface (b). Our model calculation of laser beam transfer through the sea surface is achieved by implementation of the sea surface shape as a triangular grid pattern. The dashed lines exemplify individual optical axes transferred through two of the surface triangles.

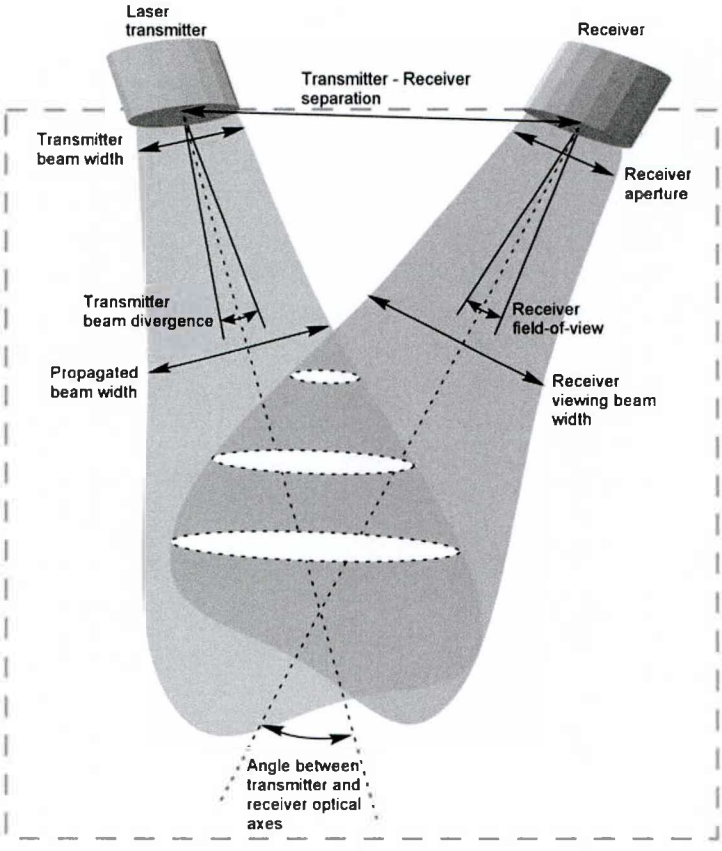

Fig. 7. Geometry and parameters for calculation of the target echo and water volume backscatter. The intersection between the transmitter and the receiver beams influences the amount of backscattered radiation from different depths in the water column.

3. Sample results of the multipixel lidar model

By separation of the lidar receiver FOV (see Fig. 5) into pixel channels and collection of the temporal impulse responses from each channel the lidar signal can be studied for different pixel geometries. We will exemplify the simulation results with the normal single pixel FOV, a 2-by-2 pixel FOV, and a 1-by-4 pixel FOV, see Fig. 8 (a)-(c). The colors of the pixels in Fig. 8 are used to make the waveform plots easy to understand in the following figures. Note in Fig. 5 and Fig. 8 that the lidar inclination angle θ_0 is in the x-z plane and that the lidar is directed forward in the x-axis direction.

In Fig. 9 we compare the simulated lidar response from a 2-by-2 and a single pixel receiver. The system and environmental parameters used are given in Table 1 and Table 2. In Fig. 9 (a) we observe that both the surface echo and the bottom echo arrive earlier, or "shallower", in the pixels that are geometrically closer to the receiver (blue and black pixels in Fig. 8) than the corresponding echoes from the red and green pixels. We can also see that each of the pixels has approximately 1/4 of the power compared to the power in the single pixel receiver, which is reasonable because the single pixel signal can be regarded as the sum of all four signals in the 2-by-2 pixel receiver. The sum of all four signals will be exactly the same as the signal in the single pixel receiver if the sea surface wave shape, where the beam hits the surface, is the same and if there is no receiver noise present. An advantage with the 2-by-2 receiver is that a temporal smearing effect of short pulses (surface and bottom echoes) can be avoided. In the following subsections we will consider the influence from surface waves, target detection, pixel geometries, and horizontally stratified water.

Table 2. Environmental parameters for simulation

Parameter	
Water	
Water attenuation coefficient c (m^{-1})	0.3
Scattering coefficient b (m^{-1})	0.15
Backscattering coefficient b_b (m^{-1})	0.006
Sea surface	
Wind-driven sea surface waves, wind speed (m/s)	3–6

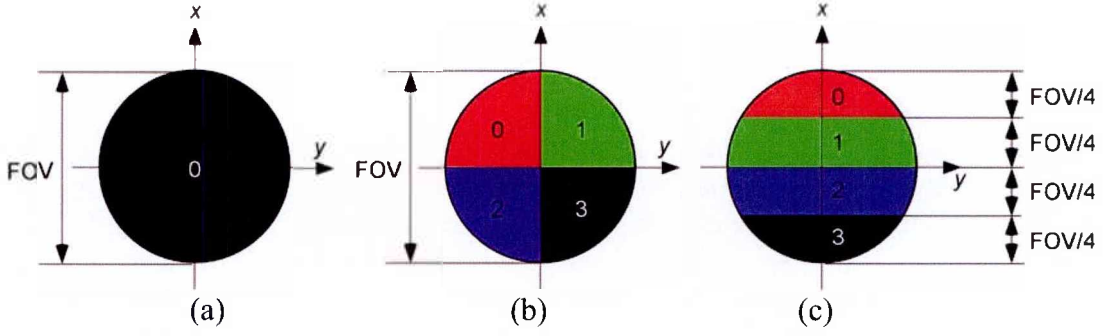

Fig. 8. Examples of FOV pixel geometries as orthogonal projections to the optical axis of the receiver.

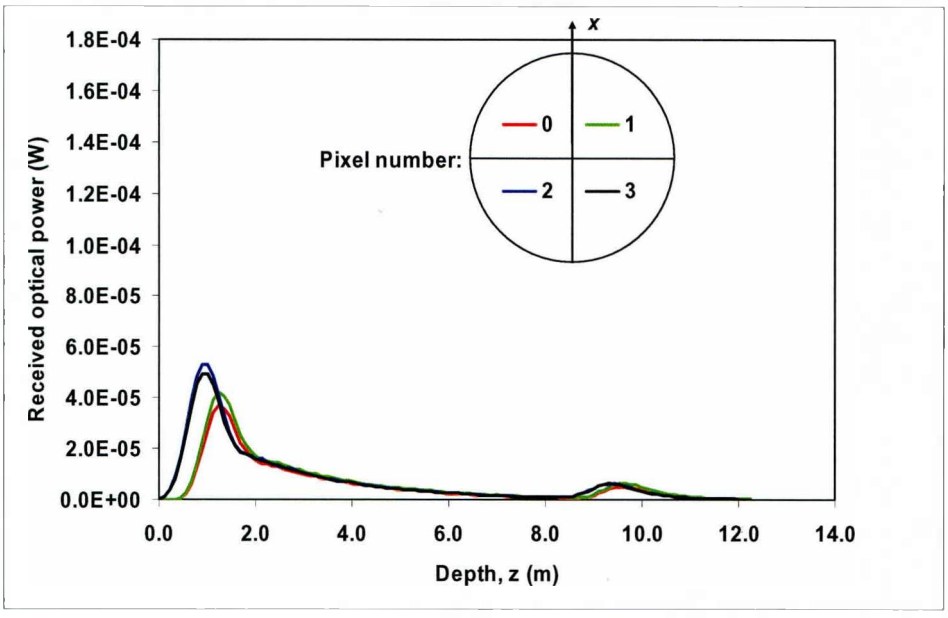

(a)

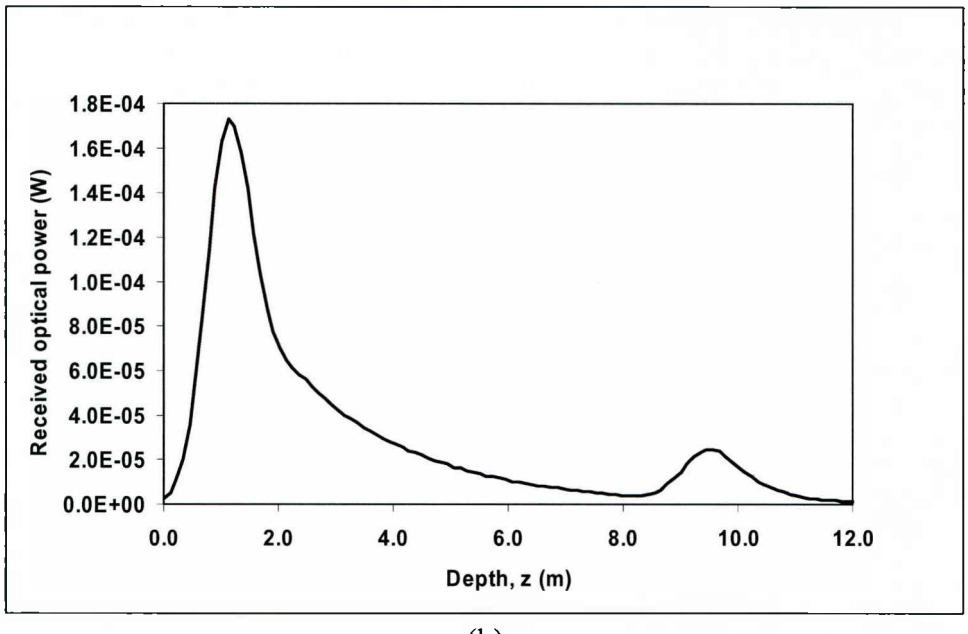

(b)

Fig. 9. Examples of model waveforms from flat bottom at 8 m depth, with 2×2 pixel (a) and single pixel receiver (b). Wind speed 3 m/s, beam divergence 10 mrad, and FOV=30 mrad. The individual pixel positions for the waveforms in (a) are shown in Fig. 8.

3.1 Sea surface waves

In Fig. 10 we show three simulated lidar shots with a 2-by-2 pixel system with the shots distributed on different positions on the sea surface slopes according to Fig. 10 (a). Details of the sea surface echo for Shots 1–3 are shown in figures (b)–(d). In Shot 1 the sea surface is sloping slightly towards the receiver and hence the surface echoes are significantly stronger (by a factor of 4–5) than the surface echoes in Shots 2–3. We can identify the possibility to estimate the local sea surface slope angle. Note e.g. that

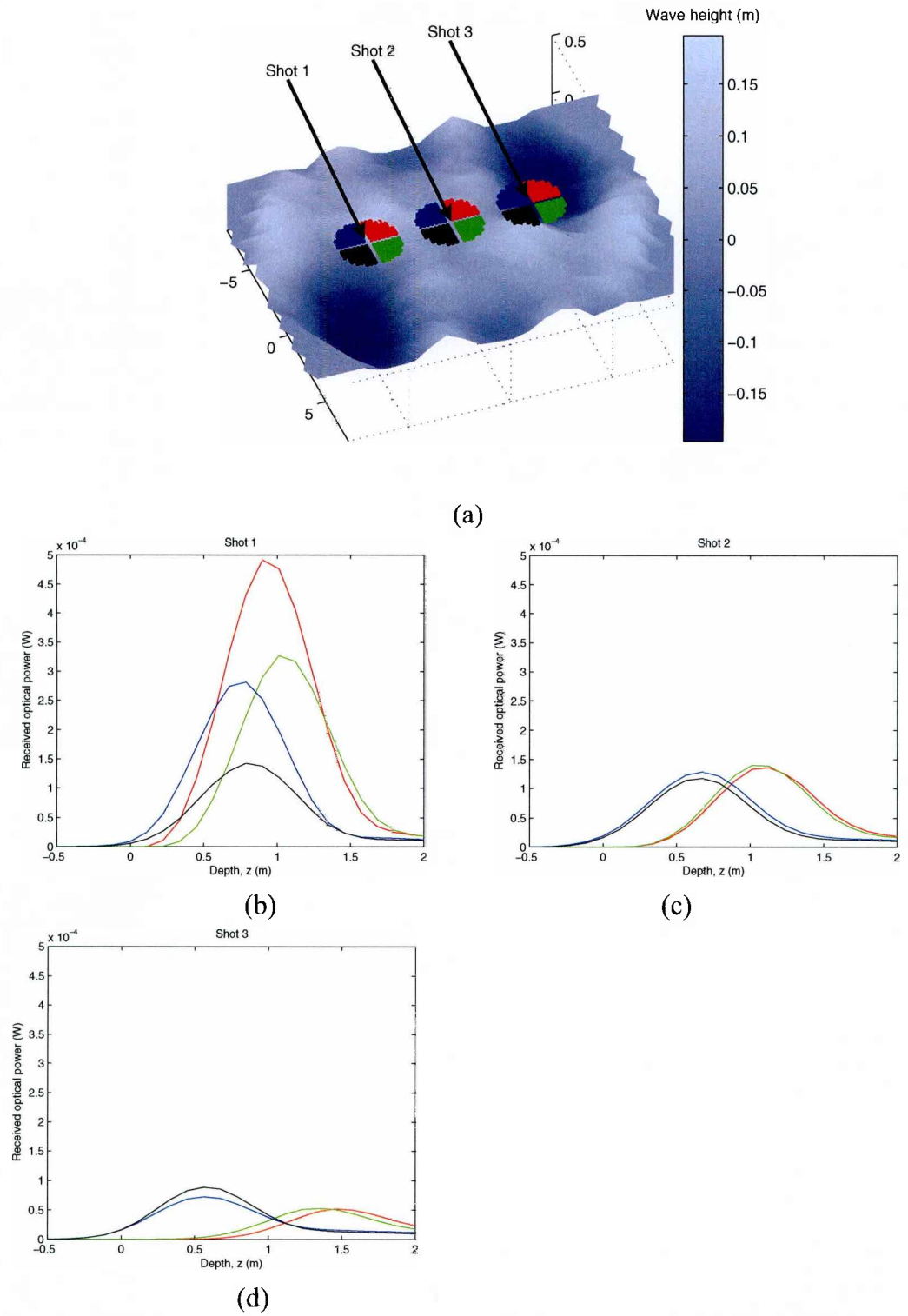

Fig. 10. Simulated lidar shot positions on a sea surface (a) and examples of simulated surface echoes with a 2×2 pixel receiver (b)-(d). Wind speed 6 m/s, beam divergence 10 mrad, and receiver FOV=15 mrad. The individual shot and pixel positions for the waveforms (red, green, blue, black) are shown in figure (a). The incidence angle $\theta_0 = 20°$ for all shots.

the four echoes in Shot 1 are more tightly grouped together, indicating a slope angle towards the receiver, than the echoes in Shot 3 where the surface normal points away from the receiver in the forward direction and thus separates the surface echoes red and green from the blue and black echoes. Note also e.g. in Shot 1 that the side sloping direction is indicated by the earlier arrival of the red-pixel echo compared to the green-pixel echo. In Shot 2, where the surface is approximately horizontal, the distance between the blue and black echoes and the red and green echoes is shorter than in Shot 3 and longer than in Shot 1.

The sea surface influences the lidar sea surface echo, but also the water volume backscatter and bottom signals are affected. In Fig. 11 we show the same three simulated lidar shots as in Fig. 10 and a detailed zoom of the bottom echo for Shots 1-3 from the red-pixel. For Shots 1 and 2 the water surface is sloping nearly towards the receiver, while for Shot 3 the surface is sloping away from the receiver in the forward direction. The simulation results in Fig. 11 (b) demonstrate that the bottom echo in Shot 3 is slightly stronger and shallower by about 0.1 m compared to the previous shots. A simple explanation to the higher intensity and the shallow bias is that the beam path in water is shorter for Shot 3, due to the refraction into a beam path close to the vertical, see Fig. 12. In practice the influence is more complex and involves scattering effects from ripples on the sea surface and within the water volume, which both are included in the simulation model.

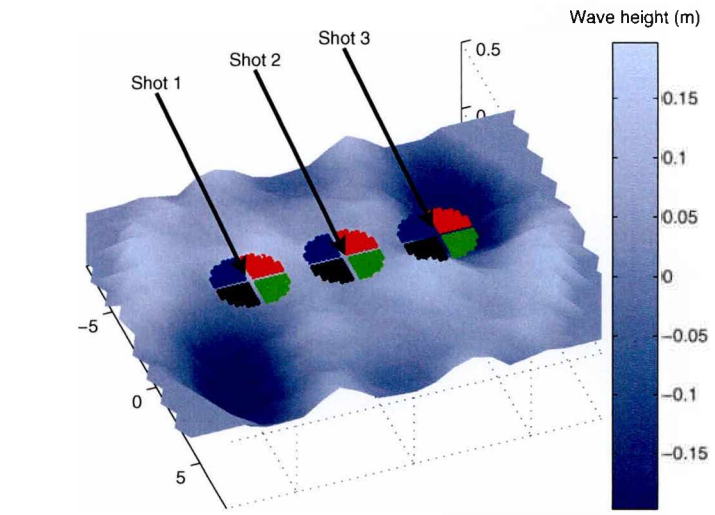

(a)

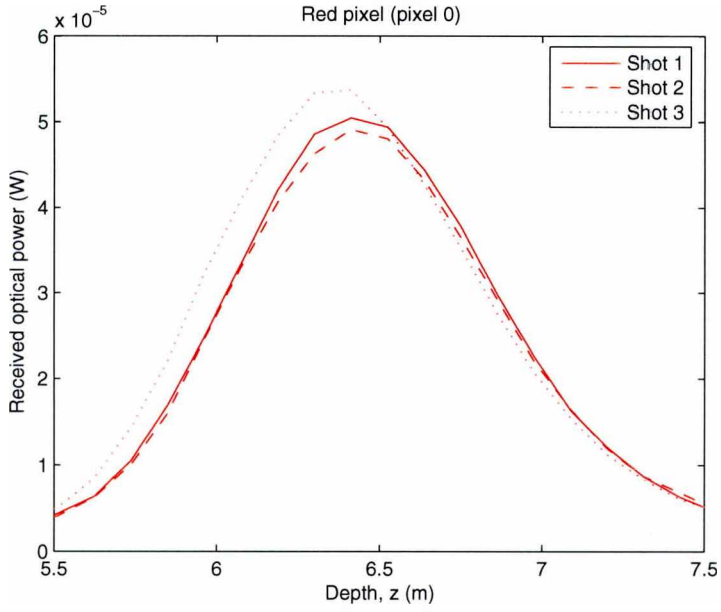

(b)

Fig. 11. Simulated lidar shot positions on a sea surface (a) and examples of simulated bottom echoes from pixel 0 (red pixel) with a 2×2 pixel receiver (b). Bottom depth is 5m, wind speed 6 m/s, beam divergence 10 mrad, and receiver FOV=15 mrad. The individual shot and pixel positions for the waveforms are shown in figure (a). The incidence angle $\theta_0 = 20°$ for all shots.

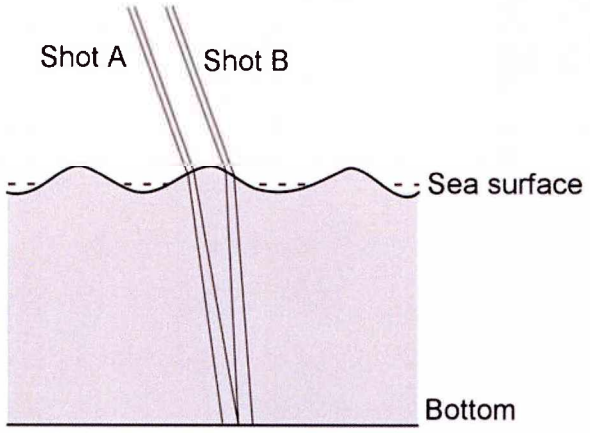

Fig. 12. Illustration of the sea surface slope influence on the beam path. In Shot A the in-water beam path between the sea surface and the bottom is longer than in Shot B.

3.2 *Target detection and different pixel geometry*

Different pixel geometries will affect the signals from targets. In Fig. 13 and Fig. 14 we compare the echo from a 1.5 m × 1.5 m target using two pixel geometries; a 2-by-2 pixel FOV, and a 1-by-4 pixel FOV, see Fig. 8 (b)-(c). Both the laser shot center position and the target center position are in $x = y = 0$. For both pixel geometries we see that the pixels closer to the receiver (blue and black), contain the largest parts of the power reflected from the target. To the left in Fig. 14, at depths smaller than 8 m, we notice that the pixels 0 (red) and 3 (black) contain much lower water volume backscatter because these pixels are on the outer parts of the transmitted beam on the sea surface, see e.g. Fig. 5. Due to the smaller FOV-areas of pixel 0 (red) and 3 (black) the signal level is therefore lower for these pixels than for the green and blue pixels. One interesting result from Fig. 14 is that the target echo in the black pixel is almost as strong as the target echo in the blue pixel, despite the smaller FOV-area and the reduced volume backscatter in the black pixel. This result can be used for improvement of target detection when the detection is limited by the volume backscatter signal, which often is the case for small targets. It should be noted that the pixel signals also depend on the relative position of the target and the laser beam. Studies of such influence must be examined with many simulation runs and is outside the scope of this report.

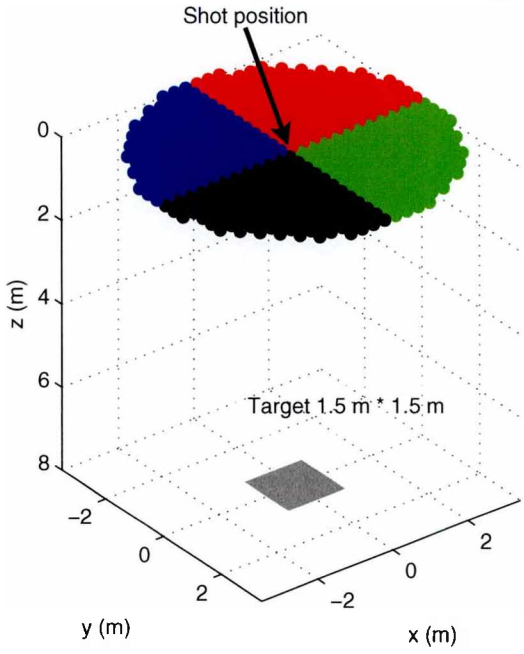

(a)

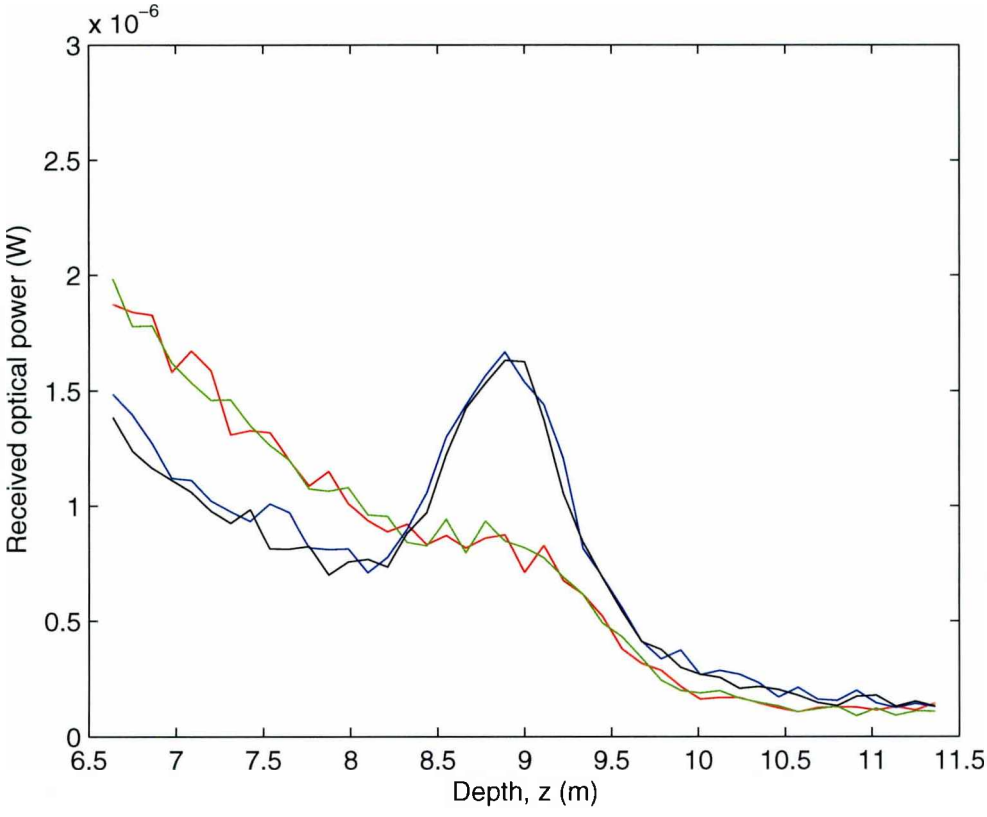

(b)

Fig. 13. Simulated lidar shot pixel positions (a) and examples of simulated target echoes with a 2×2 pixel receiver (b). The target depth is 8 m, wind speed 3 m/s, beam divergence 10 mrad, and receiver FOV=35 mrad. The individual pixel positions for the waveforms are shown in figure (a). The incidence angle $\theta_0 = 20°$.

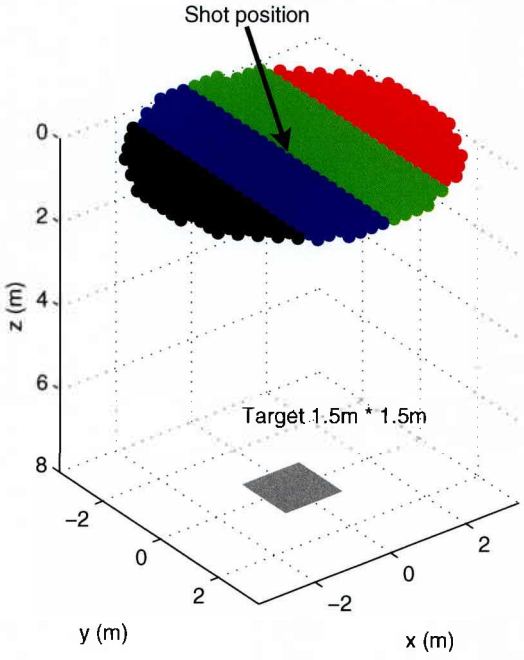

(a)

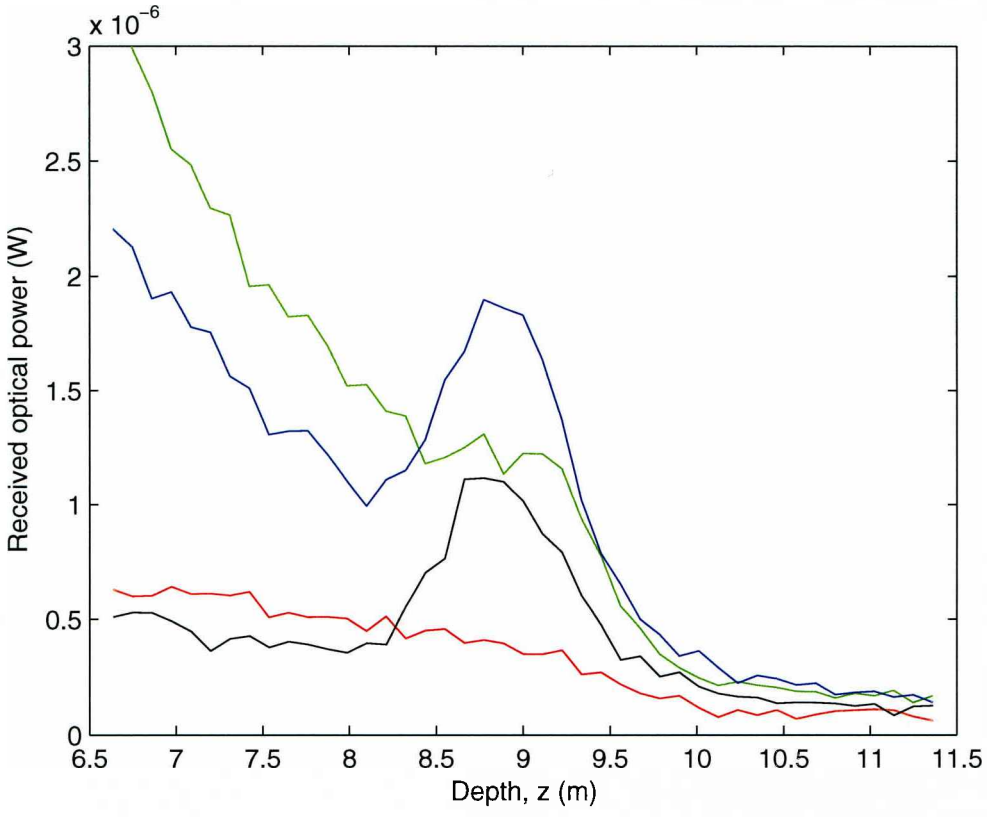

(b)

Fig. 14. Simulated lidar shot pixel positions (a) and examples of simulated target echoes with a 1x4 pixel receiver (b). The target depth is 8 m, wind speed 3 m/s, beam divergence 10 mrad, and receiver FOV=35 mrad. The individual pixel positions for the waveforms are shown in figure (a). The incidence angle $\theta_0 = 20°$.

3.3 Stratified water type

In Fig. 15 we examine the simulated lidar response from a horizontally stratified water type with a 2-by-2 and a single pixel receiver. In Fig. 15 (a) we observe that both the surface echo and the indication of stratification (at 3 m depth) arrives earlier, or "shallower", in the pixels that are geometrically closer to the receiver than the corresponding echoes from the red and green pixels. By comparing the result in detail in Fig. 16 we realize that the 2-by-2 pixel receiver has a better possibility to resolve scattering layers better than the single pixel receiver. The advantage with the 2-by-2 receiver is that a temporal smearing effect of rapid changes in the waveform can be avoided.

4. Conclusion

We have presented a model for simulation of multipixel lidar systems. The ability to simulate multipixel systems is important for performance estimation for target detection, target signature studies, estimation of surface wave signals and development of signal processing for water volume turbidity estimation or sea bottom classification. We have exemplified the results with two different receiver pixel geometries with four pixels. However, simulations can be performed with an arbitrary number of pixels and shapes of the field-of-view.

From sample simulations we have identified several system effects and signal processing methods of significance for different applications. In a multipixel system there is a possibility to estimate the local sea surface slope angle not only by the wave height data from shot to shot but also by the local slope angle within one laser shot. This information can e.g. be used for improvement of the depth sounding accuracy of the system.[5] The simulation results also show that a sea surface correction factor could be applied to improve the estimation of the sea bottom properties from the bottom echo. Another result is that the use of specific pixel information for certain pixel geometries can improve the performance for target detection when the detection is limited by the volume backscatter signal. Generally, the use of multipixel systems will improve both the horizontal and the depth resolution, which is valuable for most applications. One disadvantage with a multipixel system is the lower signal level in each pixel channel, but this disadvantage only has an impact when the signals are noise limited.

The pixel effects on depth biases and echo strength will be affected by different water turbidities. A systematic use of simulation results from the model for development of detection and signal processing methods will require many simulation runs with different water types, depths, bottom and target properties.

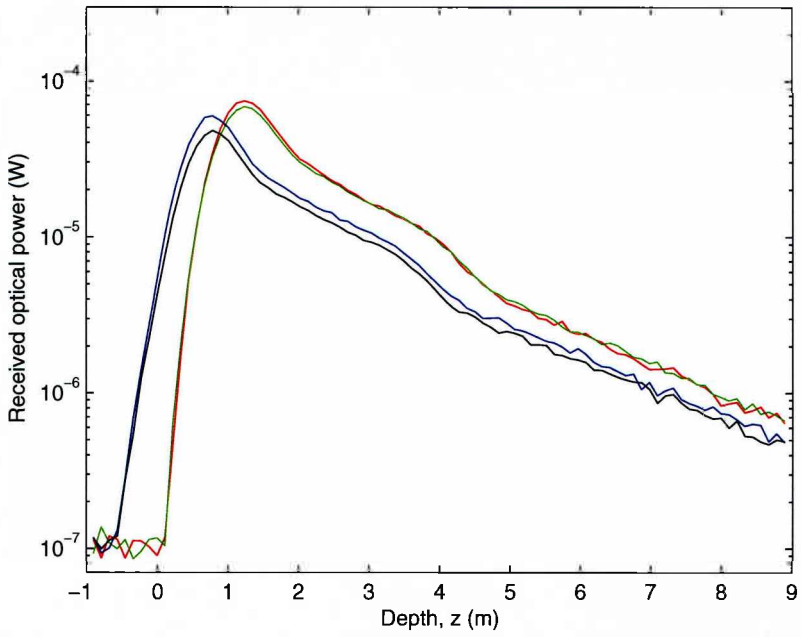

(a)

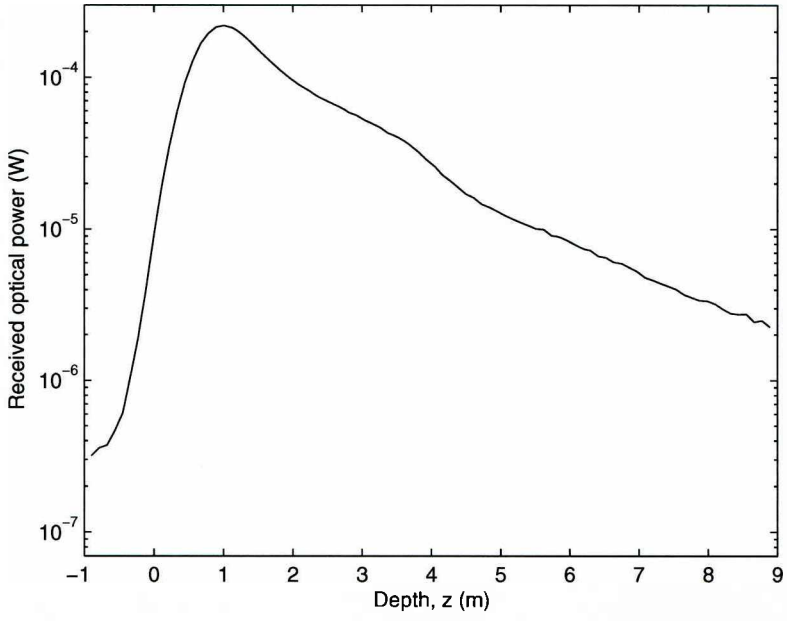

(b)

Fig. 15. Examples of model waveforms from horizontally stratified water with 2×2 pixel (a), and single pixel receiver (b). Wind speed 3 m/s, beam divergence 10 mrad, and FOV=35 mrad. The individual pixel positions for the waveforms in (a) are shown in Fig. 8. The water attenuation coefficient is c = 0.9 m^{-1} for 0-3 m depth and c = 0.5 m^{-1} for depths larger than 3 m.

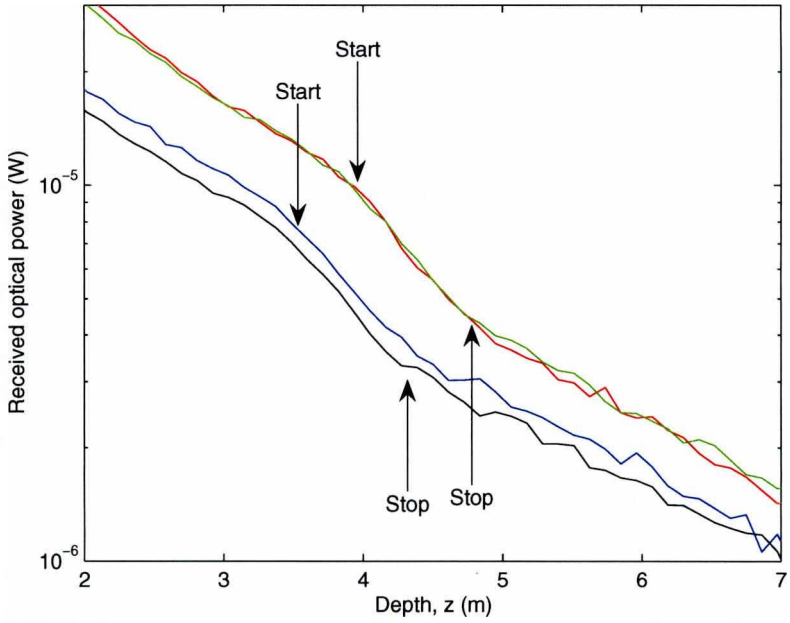

(a)

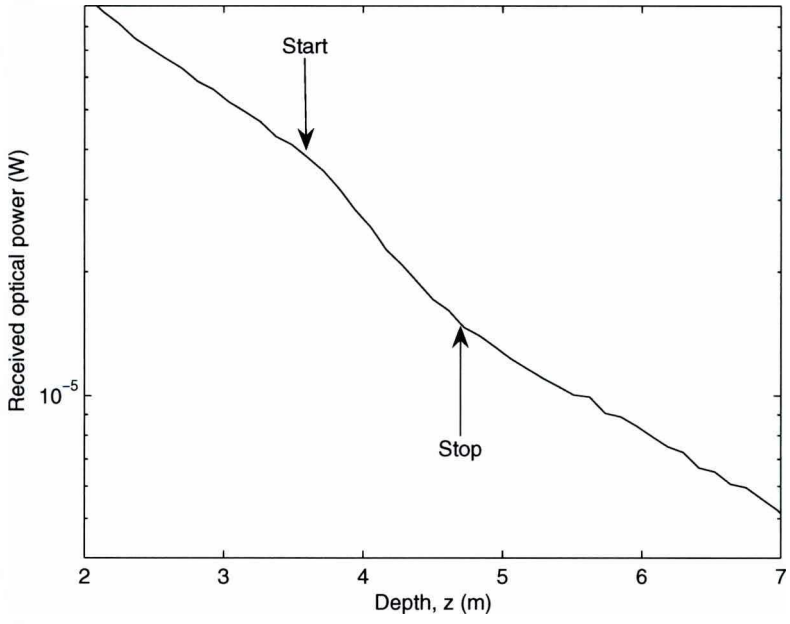

(b)

Fig. 16. Examples of model waveforms from horizontally stratified water with 2×2 pixel (a), and single pixel receiver (b). Zoom of waveforms from Fig. 15. The arrows show the start and stop of the change in the waveforms which are caused by a sudden change in the attenuation coefficient at 3 m depth. The water attenuation coefficient is c = 0.9 m^{-1} for 0-3 m depth and c = 0.5 m^{-1} for depths larger than 3 m.

5. References

[1] H. M. Tulldahl and K. O. Steinvall, "Simulation of sea surface wave influence on small target detection with airborne laser depth sounding," *Appl. Opt.* **42**(12), 2462-2483 (2004).

[2] H. M. Tulldahl, M. Andersson, and B. Knuthammar, "Detection of sea mines with airborne lidar - data analysis and results from Swedish-German sea trials," FOA Försvarets Forskningsanstalt (Defence Research Establishment) Test Report FOA-R--00-01444-409--SE (Linköping, Sweden, 2000).

[3] I. L. Katsev, E. P. Zege, A. S. Prikhach, and I. N. Polonsky, "Efficient technique to determine backscattered light power for various atmospheric and oceanic sounding and imaging systems," *J. Opt. Soc. Am.* **14**(6), 1338-1346 (1997).

[4] J. W. McLean, J. D. Freeman, and R. E. Walker, "Beam spread function with time dispersion," *Appl. Opt.* **37**(21), 4701-4711 (1998).

[5] H. M. Tulldahl, M. Andersson, and K. O. Steinvall, "Airborne laser depth sounding: Improvements in position- and depth estimates by local corrections for sea surface slopes," presented at the Oceans 2000, MTS/IEEE Conference, Providence, USA, 11-14 Sept. 2000.

FOI is an assignment-based authority under the Ministry of Defence. The core activities are research, method and technology development, as well as studies for the use of defence and security. The organization employs around 1350 people of whom around 950 are researchers. This makes FOI the largest research institute in Sweden. FOI provides its customers with leading expertise in a large number of fields such as security-policy studies and analyses in defence and security, assessment of different types of threats, systems for control and management of crises, protection against and management of hazardous substances, IT-security and the potential of new sensors.

FOI
Defence Research Agency
Systems Technology
SE-164 90 Stockholm

Phone: +46 8 555 030 00
Fax: +46 8 555 031 00

www.foi.se